# Nonlinear Time-Domain Modeling by Multiresolution Time Domain (MRTD)

Michael Krumpholz, *Member, IEEE,* Herbert G. Winful, *Member, IEEE,* and Linda P. B. Katehi, *Fellow, IEEE*

***Abstract*— A multiresolution time-domain (MRTD) scheme based on the expansion in scaling functions is applied to the modeling of nonlinear pulse propagation. Appropriate absorbers for the MRTD scheme are presented and their performance is discussed. The differences using pulse functions and nonlocalized basis functions like the Battle–Lemarie scaling functions are demonstrated by deriving time-domain schemes for both sets of orthonormal basis functions.**

***Index Terms*—Nonlinear, time domain, wavelets.**

## I. Introduction

WAVELET functions and the related concept of multiresolution analysis has become a matter of fast-growing interest in electromagnetic society. The application of wavelet expansions to the solution of integral equations leads to very sparse moment matrices and to advantages over conventional basis functions [1], [2]. Recently, it has been shown that these advantages are also present when applying wavelet expansions to the solution of differential equations. In particular, the application of multiresolution analysis directly to Maxwell's equations has lead to new multiresolution time-domain (MRTD) schemes with highly linear dispersion characteristics [3], [4]. The unparalleled inherent properties of the MRTD schemes provide advantages over the finite-difference time-domain (FDTD) scheme of [5] with respect to memory requirements and execution time. The purpose of this paper is to demonstrate that these advantages also do exist in the case of modeling nonlinear materials. While the physics of the nonlinear pulse propagation is described in detail in [6], this paper concentrates on the computational aspects of solving the nonlinear partial differential equations.

The method of moments [7] has proven to be a powerful approach not only for the numerical analysis of integral equations, but also for the discretization of partial differential equations. In particular, the application of the method of moments for the discretization of Maxwell's equations has lead to the field theoretical foundation of the transmission line method (TLM) method [8], [9]. In addition, it has been shown in [8], [10] that Yee's FDTD scheme can be derived using the same approach with pulse functions for the expansion of the unknown fields. In general, the method of moments allows for the use of any complete set of orthonormal basis functions. In [3], [4], cubic spline Battle–Lemarie scaling and wavelet functions [11], [12] have been used as expansion functions in space domain. Since the use of scaling and wavelet functions as a complete set of basis functions is called multiresolution analysis [13], [14], the resulting time-domain schemes have been called MRTD schemes. Throughout this paper, the electromagnetic fields are represented by an expansion in terms of scaling functions only, thus the resulting scheme is denoted by a S-MRTD scheme. In order to obtain a two-step S-MRTD scheme with respect to time, pulse functions are used as expansion and test functions in time domain.

While the use of localized basis functions like pulse functions allows for a localized modeling of material properties, the application of nonlocalized basis functions like the Battle–Lemarie scaling functions requires a nonlocalized modeling of material discontinuities. To illustrate the differences in the two approaches, it is at first demonstrated how to discretize the nonlinear partial differential equations using pulse functions. This approach leads to a FDTD scheme modeling the pulse compression in a nonlinear distributed optical fiber filter. In the second part of the paper, the nonlinear partial differential equations are discretized using Battle–Lemarie scaling functions instead of pulse functions. Two absorbers, absorbing boundary conditions (ABC's) based on the one-way wave equation [15] and the perfectly-matched layer (PML) technique [16] are presented and their performance is discussed for both FDTD and MRTD.

## II. Nonlinear FDTD Modeling

### A. The Derivation of the FDTD Scheme

The physical system modeled in this paper is a spatially periodic dielectric medium whose refractive index depends on the intensity of an incident electromagnetic pulse. The refractive index can be written as

$$n(z) = n_0 + n_1 \cos(2\beta_0 z) + n_2 |E|^2. \tag{1}$$

Here $n_0$ is the background refractive index, $n_1$ is the amplitude of the periodic index perturbation $(n_1 \ll n_0)$, $n_2$ is the nonlinear index coefficient, and $E$ is the electric field. Within the medium, the total field is taken as a sum of forward and

Manuscript received February 16, 1996; revised November 21, 1996.This work was supported by a scholarship from the NATO Science Committee through the German Academic Exchange Service and by the U.S. Army Research Office.

The authors are with the Department of Electrical Engineering and Computer Science, University of Michigan, Ann Arbor, MI 48109-2122 USA.

Publisher Item Identifier S 0018-9480(97)01715-8.

backward propagating waves

$$E = E_F(z, t)\exp[\jmath(\beta z - \omega t)] + E_B(z, t)\exp[-\jmath(\beta z + \omega t)] \quad (2)$$

where $\beta$ is the wavenumber of the field envelopes $E_F$ and $E_B$, which are slowly varying functions of space and time. The periodic spatial modulation of the refractive index leads to coupling between forward and backward waves, the strength of which coupling is described by the constant $k = \pi n_1/\lambda_0$, where $\lambda_0 = 2\pi n_0/\beta_0$. By using (1) and (2) in Maxwell's equations and making use of the slowly varying envelope approximation following equations for $E_F$ and $E_B$ may be obtained:

$$\frac{\partial E_F}{\partial z} + \frac{n_0}{c}\frac{\partial E_F}{\partial t} = \jmath\kappa E_B e^{-2\jmath\Delta\beta z} + \jmath\gamma(|E_F|^2 + 2|E_B|^2)E_F \quad (3)$$

$$\frac{\partial E_B}{\partial z} - \frac{n_0}{c}\frac{\partial E_B}{\partial t} = -\jmath\kappa E_F e^{2\jmath\Delta\beta z} - \jmath\gamma(|E_B|^2 + 2|E_F|^2)E_B. \quad (4)$$

The terms on the right-hand side (RHS) cubic in fields describe self-phase modulation, while the linear terms on the left-hand side (LHS) describe the dispersive coupling between the slowly varying electric-field components, the forward field $E_F$ and the backward field $E_B$. The refractive index $n_0$ represents the refractive index of the nonlinear medium without spatially periodic variation. The coupling constant $\kappa$ is directly proportional to the amplitude of the cosines variation of the refractive index, while $\gamma$ is directly proportional to the nonlinear refractive index coefficient. The detuning parameter $\Delta\beta$ is defined as the difference between the propagation constant of a guided mode and the wavenumber of the grating [6].

The forward and backward field $E_x(z, t)$ with $x = F, B$ is expanded as

$$E_x(z, t) = \sum_{k,m=-\infty}^{+\infty} E^x_{k,m} h_k(t) h_m(z) \quad (5)$$

where $E^x_{k,m}$ with $x = F, B$ are the constant expansion coefficients. The indices $m$ and $k$ are the discrete space and time indices related to the space and time coordinates via $z = m\Delta z$ and $t = k\Delta t$, where $\Delta z$ and $\Delta t$ represent the space discretization interval in $z$-direction and the time discretization interval, respectively. The function $h_m(z)$ is defined by

$$h_m(z) = h\left(\frac{z}{\Delta z} - m\right) \quad (6)$$

with the rectangular pulse function

$$h(z) = \begin{cases} 1, & \text{for } |z| < \frac{1}{2} \\ \frac{1}{2}, & \text{for } |z| = \frac{1}{2} \\ 0, & \text{for } |z| > \frac{1}{2} \end{cases}. \quad (7)$$

Then the field expansions are inserted in Maxwell's equations and the equations are sampled using pulse functions as test functions. For the sampling of the linear terms with respect to space and time, the orthogonality relation is needed

$$\int_{-\infty}^{+\infty} h_m(z) h_{m'}(z)\, dz = \delta_{m,m'}\Delta z \quad (8)$$

where $\delta_{m,m'}$ represents the Kronecker symbol

$$\delta_{m,m'} = \begin{cases} 1, & \text{for } m = m' \\ 0, & \text{for } m \neq m' \end{cases}. \quad (9)$$

Using

$$\int_{-\infty}^{+\infty} \delta(z - z_0) f(z)\, dz = f(z_0) \quad (10)$$

and

$$\frac{\partial h(z)}{\partial z} = \delta\left(z + \frac{1}{2}\right) - \delta\left(z - \frac{1}{2}\right) \quad (11)$$

yields

$$\int_{-\infty}^{+\infty} h_m(z)\frac{\partial h_{m'}(z)}{\partial z}\, dz = \frac{1}{2}(\delta_{m+1,m'} - \delta_{m-1,m'}). \quad (12)$$

The later integral is needed for the sampling of the derivatives with pulse functions in both space and time domains.

The nonlinear terms are discretized in a consistent manner, which indicates the need to calculate the integrals

$$\int_{-\infty}^{+\infty} h_m(z) h_{m'}(z) e^{\pm 2\jmath\Delta\beta z}\, dz = \delta_{m,m'}\Delta z \frac{\sin\Delta\beta\Delta z}{\Delta\beta\Delta z} e^{\pm 2\jmath\Delta\beta m\Delta z} \quad (13)$$

in order to discretize the first nonlinear term on the RHS of (1) and (2). For the second term on the RHS, the intensities $|E_F|^2$ and $|E_B|^2$ have to be expressed in terms of the expansion coefficients. The field expansions (3) as well as the orthogonality relations (5), are used to calculate

$$|E_x(z, t)|^2 = \sum_{k,k',m,m'=-\infty}^{+\infty} E^x_{k,m} E^x_{k',m'} \int_{-\infty}^{+\infty}\int_{-\infty}^{+\infty} \cdot h_k(t) h_{k'}(t) h_m(z) h_{m'}(z)\, dt\, dz = \sum_{k,m=-\infty}^{+\infty} \Delta t\Delta z |E^x_{k,m}|^2 \quad (14)$$

where again $x = F, B$. The scalar $\Delta t\Delta l|E^x_{k,m}|^2$ represents the energy in one space and time discretization interval at $t = k\Delta t$ and $z = m\Delta z$. Thus, the intensity for this discretization interval is given by $|E^x_{k,m}|^2$. Proceeding as described in [8], [10], the authors obtain the partial difference equations

$$\begin{aligned} E^F_{k+1,m} - E^F_{k-1,m} + s(E^F_{k,m+1} - E^F_{k,m-1}) &= 2\jmath\kappa s\Delta z \frac{\sin\Delta\beta\Delta z}{\Delta\beta\Delta z} E^B_{k,m} e^{-2\jmath\Delta\beta m\Delta z} \\ &\quad + 2\jmath\gamma s\Delta z(|E^F_{k,m}|^2 + 2|E^B_{k,m}|^2)E^F_{k,m} \\ E^B_{k+1,m} - E^B_{k-1,m} - s(E^B_{k,m+1} - E^B_{k,m-1}) &= 2\jmath\kappa s\Delta z \frac{\sin\Delta\beta\Delta z}{\Delta\beta\Delta z} E^F_{k,m} e^{2\jmath\Delta\beta m\Delta z} \\ &\quad + 2\jmath\gamma s\Delta z(|E^B_{k,m}|^2 + 2|E^F_{k,m}|^2)E^F_{k,m} \end{aligned} \quad (15)$$

where 5 is the stability factor $s = c\Delta t/(n_0\Delta l)$.

### *B. Boundary Conditions for the FDTD Scheme*

For the optical fiber filter, the boundary conditions at the beginning of the nonlinear material at $z = 0$ and at the end of the nonlinear material at $z = L$ are given by

$$E_F(0, t) = \sqrt{\frac{A}{2}}(1 + j)e^{-t^2/(2\alpha^2)} \tag{16}$$

implying an intensity of

$$|E_F(0, t)|^2 = Ae^{-t^2/\alpha^2} \tag{17}$$

and

$$E_B(L, t) = 0 \tag{18}$$

as well as

$$\left.\frac{\partial E_B}{\partial z}\right|_{z=0} = \frac{n_0}{c}\left.\frac{\partial E_B}{\partial t}\right|_{z=0} \tag{19}$$

and

$$\left.\frac{\partial E_F}{\partial z}\right|_{z=L} = -\frac{n_0}{c}\left.\frac{\partial E_F}{\partial t}\right|_{z=L}. \tag{20}$$

While the implementation of the boundary conditions (16) and (18) is straightforward, (19) and (20) require special care. One way of satisfying the radiating boundary conditions is to choose an ABC based on the one-way wave equation similar to the ABC's presented in [15] for two-dimensional (2-D) FDTD. Assuming integer values for the stability factor $s$, $E^B_{k,0}$ is determined by the backward field at $z = \Delta z$, $E^B_{k,1}$, by

$$E^B_{k,0} = E^B_{k-1/s,1} \tag{21}$$

and $E^F_{k,L/\Delta z}$ by the forward field at $z = L - \Delta z$, $E^B_{k,L/\Delta z-1}$, by

$$E^F_{k,L/\Delta z} = E^F_{k-1/s,L/\Delta z-1}. \tag{22}$$

Another way of satisfying the radiating boundary conditions is to use the PML technique [16]. Note that for the one-dimensional (1-D) case, this absorber reduces to a physical absorbing layer. The absorbing material with the permittivity $\varepsilon_0$ and the conductivity $\sigma$ is described by the partial differential equations

$$\frac{1}{c}\frac{\partial E_x}{\partial t} \pm \frac{\partial E_x}{\partial z} + \sigma' E_x = 0 \tag{23}$$

where $\sigma' = \sigma/(\varepsilon_0 c)$ and where again $x = F, B$. As mentioned in [16], a direct discretization of (23) leads to numerical reflections due to sharp variations of the conductivity. Substituting

$$E_x(z, t) = \tilde{E}_x(z, t)e^{-\sigma' t} \tag{24}$$

leads to the homogeneous one-way wave equation for $\tilde{E}_x(z, t)$ in free space

$$\frac{1}{c}\frac{\partial \tilde{E}_x}{\partial t} \pm \frac{\partial \tilde{E}_x}{\partial z} = 0. \tag{25}$$

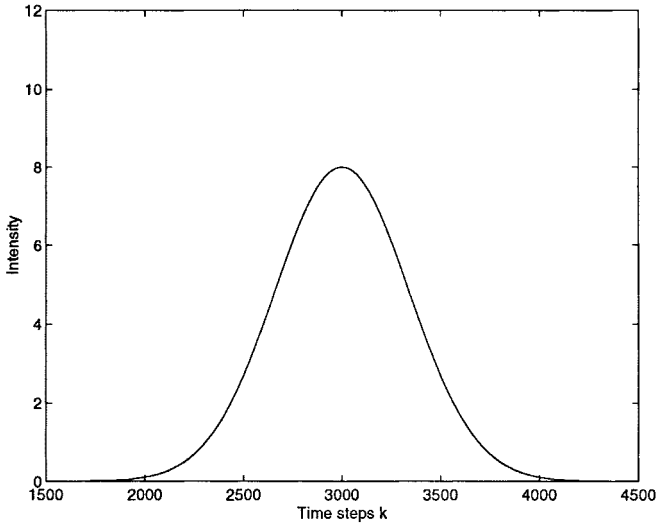


Fig. 1. Transmitted pulse modeled by FDTD.

Thus the absorbing material may be modeled by

$$E^x_{k+1,m} = e^{-2\sigma'\Delta t}E^x_{k-1,m} \mp se^{-\sigma'\Delta t}(E^x_{k,m+1} - E^x_{k,m-1}). \tag{26}$$

Note that a correct discretization using the method of moments requires the separate discretization of (24) and (25) using the integral

$$\int_{-\infty}^{+\infty} h_k(t)h_{k'}(t)e^{-\sigma' t}\,dt = \delta_{k,k'}\Delta t\,\frac{\sinh\left(\frac{\sigma'\Delta t}{2}\right)}{\frac{\sigma'\Delta t}{2}}\,e^{-\sigma' k\Delta t}. \tag{27}$$

Sampling (24) in space domain, the conductivity is assumed in terms of pulse functions with respect to space. To obtain (26), one has to eliminate $\tilde{E}^x_{k,m}$ and use the approximation $\sinh x/x \approx 1$ for $x \to 0$, which is justified since the values of $\sigma'\Delta t$ are small. For all simulations, a parabolic distribution of the conductivity in the absorbing layer is used with the thickness $N\Delta z$

$$\sigma'(m\Delta z) = \sigma_0\left(\frac{m}{N}\right)^2, \qquad \text{for } m = 0, 1, \cdots, N \tag{28}$$

where $\sigma_0$ represents the maximum of the conductivity at the end of the absorbing layer. As in [16], the FDTD mesh is terminated by a perfect electric conductor (PEC) at the end of the absorbing layer.

Choosing a Gaussian excitation according to (16) with $A = 8$ and $\alpha = 480/\Delta t$ as shown in Fig. 1, the intensity $|E_F(z, t)|^2$ of the transmitted pulse is calculated by the FDTD scheme as shown in Fig. 2. For the simulation, (1) and (2) have been normalized in terms of the length of the nonlinear material $L$ and the transient time $\tau$. The parameters have then been chosen to be $\tau = n_0 L/(10c)$ as well as

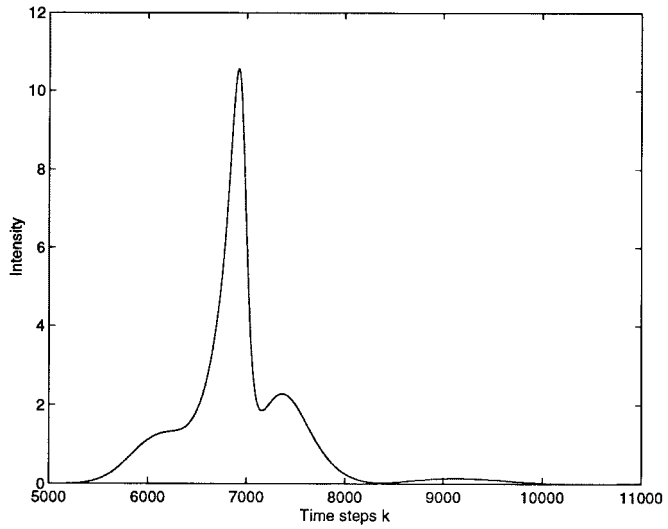


Fig. 2. Incident Gaussian pulse.

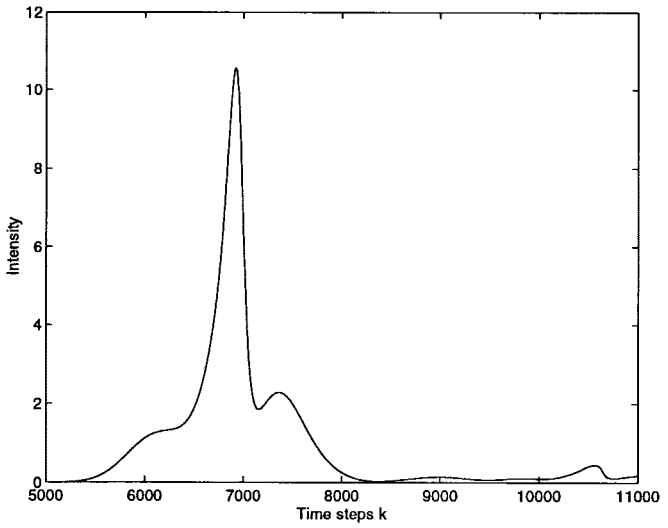


Fig. 3. Transmitted pulse modeled by FDTD with reflections from the absorbers.

TABLE I
THE PEAK VALUES OF THE INTENSITY OF THE TRANSMITTED PULSE

| $L/\Delta z$ | FDTD | MRTD |
|---|---|---|
| 100 | | 10.407 |
| 200 | 7.969 | 10.623 |
| 500 | 10.189 | |
| 1000 | 10.562 | |

$\kappa L = 4$, $\beta L = 12$, and $\gamma L = 2/3$. With this choice of the parameters, the results obtained by integrating numerically along the forward and backward characteristics [6] could be reproduced. As for the discretization, for the results shown in Fig. 2, a space and time discretization interval of $\Delta z = 0.001$ and $\Delta t = 0.003\,125$ was chosen, thus the nonlinear material was modeled by a mesh with 1000 grid points. With half of the grid points, the transient pulse starts to be distorted and is, therefore, not modeled correctly anymore. Table I gives the peak values of the intensity of the transmitted pulse for modeling the nonlinear material by a mesh with 200, 500, and 1000 grid points. Both suggested absorbers, the ABC based on the one-way wave equation and the PML technique have been applied in the FDTD simulation. The ABC requires much less computational efforts than the PML technique, however, it is unstable in the nonlinear simulation. Therefore, the preferred ABC for the nonlinear simulation is the PML technique. For Fig. 2, a parabolic distribution of the conductivity according to (28) with $N = 1000$ and $\sigma_0 = 0.1$ has been used. On a first view, the value of $N = 1000$ seems to be very large, however, Fig. 3 illustrates that some reflections from the absorber superimposes with the transmitted pulse, when the thickness of the absorbing layer is reduced by a factor of two and when $N = 500$ is chosen instead. Note that for an absorbing layer with $N = 500$, increasing $\sigma_0$ increases the reflections of the absorber due to the sharp variations of the conductivity and decreasing $\sigma_0$ increases the reflections of the absorber because the conductivity is not high enough to absorb the pulse completely.

## III. NONLINEAR MRTD MODELING

### A. The Derivation of the S-MRTD Scheme

For the derivation of the S-MRTD scheme, the fields are expanded in

$$E_x(z, t) = \sum_{k,m=-\infty}^{+\infty} E_{k,m}^{y} h_k(t)\phi_m(z) \tag{29}$$

where $E_{k,m}^{y}$ with $y = f,\ b$ are the constant expansion coefficients for the scaling function expansions. The function $\phi_m(z)$ is defined as

$$\phi_m(z) = \phi\Big(\frac{z}{\Delta z} - m\Big) \tag{30}$$

where $\phi(z)$ represents the cubic spline Battle–Lemarie scaling functions [11], [12] depicted in Fig. 4. Assuming a Fourier transformation defined by

$$\tilde{\phi}(\lambda) = \int_{-\infty}^{+\infty} \phi(z) e^{\jmath\lambda z}\, dz \tag{31}$$

and

$$\phi(z) = \frac{1}{2\pi} \int_{-\infty}^{+\infty} \tilde{\phi}(\lambda) e^{-\jmath\lambda z}\, d\lambda \tag{32}$$

the closed-form expression of the scaling function in spectral domain is given by [17] as shown in (33) at the bottom of the next page, with the low-pass spectral domain characteristics shown in Fig. 5.

Then, the field expansions are inserted in (1) and the equations are sampled using pulse functions as test functions in time and scaling functions as test functions in space. The sampling with respect to time is the same as for the derivation of the FDTD scheme. For the sampling with respect to space, the authors use the orthogonality relation for the scaling functions [17]

$$\int_{-\infty}^{+\infty} \phi_m(z)\phi_{m'}(z)\, dz = \delta_{m,m'}\Delta z. \tag{34}$$

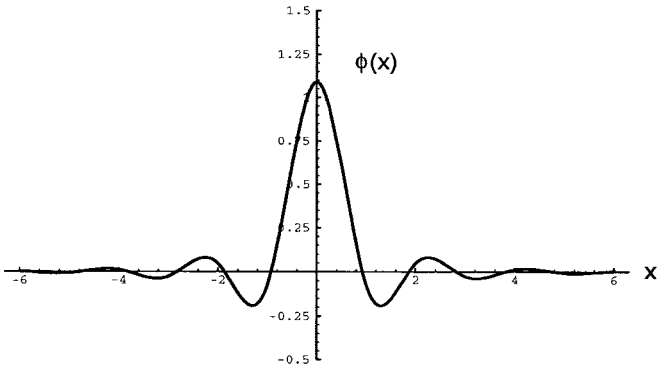


Fig. 4. Cubic spline Battle–Lemarie scaling function in space domain.

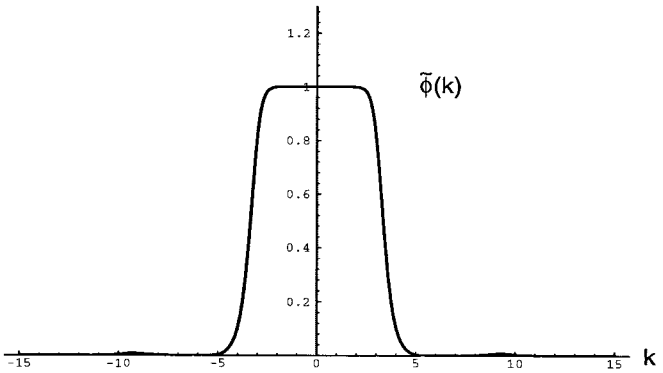


Fig. 5. Cubic spline Battle–Lemarie scaling function in spectral domain.

To calculate the integral corresponding to (10) for scaling functions, the closed-form expression of the scaling function in the spectral domain is used. According to Galerkin's method [7], for complex basis functions, one has to choose the complex conjugant of the basis functions as test functions. Then, the integral is obtained

$$\int_{-\infty}^{+\infty} \phi_m(z)\,\frac{\partial \phi_{m'}(z)}{\partial z}\,dz = \frac{1}{\pi}\int_0^{\infty} |\tilde{\phi}(\lambda)|^2 \lambda \sin\,\lambda(m'-m)\,d\lambda \tag{35}$$

where $\tilde{\phi}(\lambda)$ is given by (33). This integral may be evaluated numerically resulting in

$$\int_{-\infty}^{+\infty} \phi_m(z)\,\frac{\partial \phi_{m'}(z)}{\partial z}\,dz = \sum_{i=-\infty}^{+\infty} a(i)\delta_{m+i,\,m'}. \tag{36}$$

The coefficients $a(i)$ for $0 \le i \le 15$ are shown in Table II, the coefficients $a(i)$ for $i < 0$ are given by the symmetry relation $a(-i) = -a(i)$. The Battle–Lemarie scaling function does not have compact, but only exponential, decaying support and thus the coefficients $a(i)$ for $i > 15$ are not zero. However, these coefficients are negligible and do not affect the accuracy of the nonlinear MRTD modeling, thus the approximation is used

TABLE II
THE COEFFICIENTS $a(i)$

| $i$ | $a(i)$ |
|---|---|
| 0 | 0.0 |
| 1 | 0.9410963 |
| 2 | –0.3946688 |
| 3 | 0.2000380 |
| 4 | –0.1057210 |
| 5 | 0.0564244 |
| 6 | –0.0301826 |
| 7 | 0.0161536 |
| 8 | –0.0086464 |
| 9 | 0.0046282 |
| 10 | –0.0024774 |
| 11 | 0.0013261 |
| 12 | –0.0007098 |
| 13 | 0.0003780 |
| 14 | –0.0002092 |
| 15 | 0.0001085 |

$$\int_{-\infty}^{+\infty} \phi_m(z)\,\frac{\partial \phi_{m'}(z)}{\partial z}\,dz \approx \sum_{i=-15}^{+15} a(i)\delta_{m+i,\,m'}. \tag{37}$$

For the discretization of the nonlinear terms, the integrals have to be evaluated

$$I_{m,\,m'} = \int_0^L \phi_m(z)\phi_{m'}(z)\,dz \tag{38}$$

and

$$I^{\pm}_{m,\,m'} = \int_0^L \phi_m(z)\phi_{m'}(z)e^{\pm 2j\Delta\beta z}\,dz. \tag{39}$$

Note that as for the expansion in terms of pulse functions, the energy in terms of the scaling-function expansion coefficients is given by

$$|E_x(z,\,t)|^2 = \sum_{k,\,m=-\infty}^{+\infty} \Delta t\Delta z |E^y_{k,\,m}|^2 \tag{40}$$

where again $x = F,\ B$ and $y = f,\ b$. Thus the intensity for a discretization interval at $t = k\Delta t$ and $z = m\Delta z$ is given by $|E^y_{k,\,m}|^2$. The evaluation of the integrals $I_{m,\,m'}$ and $I^{\pm}_{m,\,m'}$ is split into three parts: the first part $m,\,m' \approx 0$, signifies close to the beginning of the nonlinear material, the

$$\tilde{\phi}(\lambda) = \left(\frac{\sin\,\frac{\lambda}{2}}{\frac{\lambda}{2}}\right)^4 \frac{1}{\sqrt{1 - \frac{4}{3}\sin^2\left(\frac{\lambda}{2}\right) + \frac{2}{5}\sin^4\left(\frac{\lambda}{2}\right) - \frac{4}{315}\sin^6\left(\frac{\lambda}{2}\right)}} \tag{33}$$

TABLE III
THE COEFFICIENTS $B_i$

| $i$ | $B_i$ |
|---|---|
| 0 | 1.9697616 |
| 1 | –0.6724304 |
| 2 | 0.2687042 |
| 3 | –0.1185199 |
| 4 | 0.0551914 |
| 5 | –0.0265203 |
| 6 | 0.0129981 |
| 7 | –0.0064574 |
| 8 | 0.0032398 |
| 9 | –0.0016377 |

second part $m, m' \approx L/\Delta z$, signifies close to the end of the nonlinear material, and the third part is the nonlinear material in between. As for the modeling of anisotropic dielectric media [4], the integrals (38) and (39) give rise to a linear matrix equation. However, this matrix contains only significant off-diagonal elements close to the beginning and the end of the nonlinear material. In between, the off-diagonal elements can be neglected, thus for $0 \ll m, m' \ll L/\Delta z$, the following is considered:

$$I_{m,m'} \approx \delta_{m,m'} \Delta z \tag{41}$$

and

$$I^{\pm}_{m,m'} \approx \delta_{m,m'} \Delta z e^{\pm 2\jmath \Delta\beta m \Delta z}. \tag{42}$$

For $m, m' \approx 0$, the integrals $I_{m,m'}$ and $I^{\pm}_{m,m'}$ are evaluated numerically using the representation of the scaling function in terms of cubic spline functions [2]. The cubic spline Battle–Lemarie scaling function in space domain may be expressed as

$$\phi(z) = \sum_{i=-\infty}^{+\infty} B_i B(z-i) \tag{43}$$

where the cubic spline function $B(z)$ is defined as

$$B(z) = \begin{cases} \dfrac{2}{3} - z^2 + \dfrac{|z|^3}{2}, & \text{for } |z| \le 1 \\ \frac{1}{6}(2-|z|)^3, & \text{for } 1 < |z| \le 2 \\ 0, & \text{for } |z| > 2 \end{cases}. \tag{44}$$

Table III gives the expansion coefficients $B_i$ which the authors have considered for the numerical evaluation of the integrals, while the coefficients $B_i$ for $i > 9$ were neglected. The coefficients $B_i$ for $i < 0$ are given by the symmetry relation $B_i = B_{-i}$. For the MRTD simulations in this paper, the integrals $I_{m,m'}$ and $I^{\pm}_{m,m'}$ close to the beginning and the end of the nonlinear material are approximated by $9 \times 9$ matrices assuming a discretization, where the maxima of the scaling functions at the beginning and the end of the nonlinear material are placed exactly at $z = 0$ and $z = L$. Note that due to the symmetry relations

$$I_{L/\Delta z - m, L/\Delta z - m'} = I_{m,m'} \tag{45}$$

as well as

$$I^{\pm}_{L/\Delta z - m, L/\Delta z - m'} = I^{\mp}_{m,m'} e^{\pm 2\jmath \Delta\beta L} \tag{46}$$

and

$$I^{\mp}_{m,m'} = (I^{\pm}_{m,m'})^* \tag{47}$$

where $(I^{\pm}_{m,m'})^*$ represents the conjugate complex of $I^{\pm}_{m,m'}$, only one matrix representing $I_{m,m'}$ and one representing $I^{\pm}_{m,m'}$ have to be calculated. Proceeding as described in [4], the partial difference equations are obtained

$$\begin{aligned} &E^f_{k+1,m} - E^f_{k-1,m} + s\mathbf{D}_z(E^f_{k,m}) \\ &\quad = 2\jmath\kappa s\Delta z \sum_{m'} I^{-}_{m,m'} E^b_{k,m'} \\ &\qquad + 2\jmath\gamma s\Delta z \sum_{m'} I_{m,m'}(|E^f_{k,m'}|^2 + 2|E^b_{k,m'}|^2) E^f_{k,m'} \\ &E^b_{k+1,m} - E^b_{k-1,m} - s\mathbf{D}_z(E^b_{k,m}) \\ &\quad = 2\jmath\kappa s\Delta z \sum_{m'} I^{+}_{m,m'} E^f_{k,m'} \\ &\qquad + 2\jmath\gamma s\Delta z \sum_{m'} I_{m,m'}(|E^b_{k,m'}|^2 + 2|E^f_{k,m'}|^2) E^f_{k,m'} \end{aligned} \tag{48}$$

where the operator has been introduced

$$\mathbf{D}_z(E^y_{k,m}) = \sum_{i=-15}^{+15} a(i) E^y_{k,m+i}. \tag{49}$$

### *B. Boundary Conditions for the MRTD Scheme*

Since the MRTD scheme is based on the expansions of the fields in terms of nonlocalized basis functions, the implementation of the boundary conditions (16) and (18) is not as straightforward as for FDTD. The boundary condition (18) requires the backward field to be zero, which is the same as considering a PEC at $z = L$ for the backward field only. Since the two partial differential equations (1) and (2) decouple for linear materials, is satisfied (18) by adding a slice of free space terminated with a PEC for the backward field only to the end of the nonlinear material. Then the image principle [3], [4] is applied to model the PEC at $z = M\Delta z$, which is equivalent to terminating the mesh at $z = M\Delta z$ and making use of the symmetry relation

$$E^f_{k,M+m} = -E^f_{k,M-m} \tag{50}$$

for the expansions coefficients outside the mesh. This procedure allows the author to use (48) without any modifications.

With respect to space domain, the forward and backward fields are represented in terms of scaling functions, thus an excitation of $E^f_{k,m}$ implies the excitation of a scaling function in space domain. In order to be able to use a pulse excitation with respect to space and to obtain an excitation identical to an FDTD excitation, the boundary condition (16) is represented in terms of a pulse function by

$$E_F(z,t)|_{\text{Boundary}} = E_F(0,t) h_0(z) \tag{51}$$

TABLE IV
THE COEFFICIENTS $c(i)$

| $i$ | $c(i)$ |
|---|---|
| 0 | 0.9150343 |
| 1 | 0.0382121 |
| 2 | 0.0096737 |
| 3 | −0.0087043 |
| 4 | 0.0050851 |
| 5 | −0.0027142 |
| 6 | 0.0014106 |

and the latter equation is discretized in terms of scaling functions. Using

$$\int_{-\infty}^{+\infty} h_m(z)\phi_{m'}(z)\,dz \approx \sum_{i=-6}^{+6} c(i)\delta_{m+i,m'}\Delta z \qquad (52)$$

where the coefficients $c(i)$ are given in Table IV and the coefficients $c(i)$ for $i<0$ by the symmetry relation $c(-i)=c(i)$, the representation of the pulse function at $z=0$ in terms of scaling functions is obtained:

$$E^f_{k,m}|_{\text{Boundary}} \approx E_F(0,\,k\Delta t)\sum_{i=-6}^{+6} c(i)\delta_{i,m} = E_F(0,\,k\Delta t)c(m), \qquad \text{for } |m|\le 6. \quad (53)$$

The forward field given by the boundary condition for $z<1/2$ is superimposed to the forward field for $z>1/2$ and the pulse excitation is modeled by

$$E^f_{k,m}|_{\text{total}} = E_F(0,\,k\Delta t)c(m) + E^f_{k,m}[1-c(m)], \qquad \text{for } |m|\le 6. \quad (54)$$

In the simulation, the forward field is calculated only for $m\ge 0$. To apply the operator defined by (49), the authors assume the forward field to be even with respect to $z=0$ so that the expansion coefficients for $m<0$ are given by

$$E^f_{k,-m} = E^f_{k,m}. \qquad (55)$$

Note that this procedure of modeling sources allows for the modeling of an arbitrary space distribution of the excitation.

The implementation of the boundary conditions (19) and (20) is straightforward for MRTD applying the ABC or the PML technique derived for the FDTD scheme. While for FDTD, an ABC determines only the field component at the boundary of the mesh, for MRTD terminating the mesh with an ABC requires the estimation of several field components beyond the boundary of the mesh. For the S-MRTD scheme used in this paper, fifteen field components have to be determined in order to use the operator defined by (49). From (21) and (22), the following equations are obtained:

$$E^B_{k,m} = E^B_{k-m/s,\,1}, \qquad \text{for } m\le 0 \qquad (56)$$

and

$$E^F_{k,m} = E^F_{k-(m-L/\Delta z)/s,\,L/\Delta z-1}, \qquad \text{for } m\ge L/\Delta z \quad (57)$$

for the ABC's at $z=0$ and $z=L$. To apply the PML technique for the termination of the MRTD mesh, the authors assume that the conductivity is given in terms of scaling functions with respect to space. Then the partial difference equations for modeling the absorbing material may be derived in the same way as described for FDTD yielding

$$E^y_{k+1,m} = e^{-2\sigma'\Delta t}E^y_{k-1,m} \mp s e^{-\sigma'\Delta t}\mathbf{D}_z(E^y_{k,m}). \qquad (58)$$

Again, (28) is used as the distribution of the conductivity in the absorbing layer, which means the amplitudes of the scaling functions $\sigma'(m\Delta z)$ have a parabolic distribution in space domain. The PEC at the end of the absorbing layer is again modeled by the image principle as discussed above.

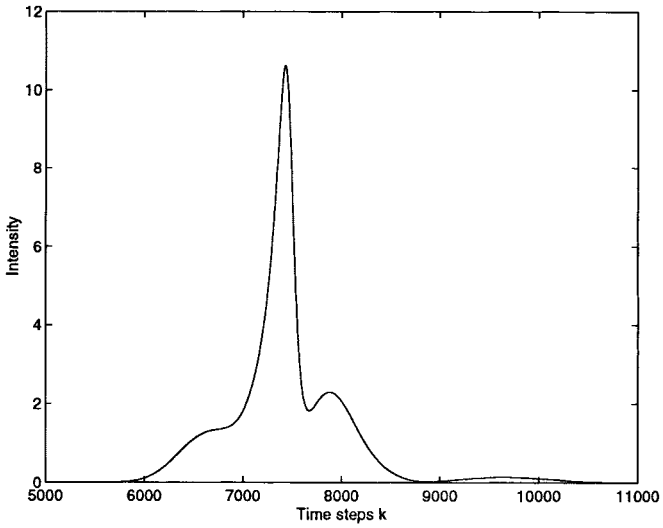


Fig. 6. Transmitted pulse modeled by MRTD.

Fig. 6 illustrates the results of the nonlinear modeling using the S-MRTD scheme. The intensity $|E_x(z,\,t)|^2$ may be obtained from the expansion coefficients $E^y_{k,m}$ by sampling the field expansions (29) with either delta functions [4] or with pulse functions. Since the results of the MRTD simulation will be compared to the FDTD results, (29) is sampled with pulse functions and

$$E_x(z_0,\,t_0) = \iint E_x(z,\,t)h(z-m\Delta z)h(t-k\Delta t)\,dz\,dt \approx \sum_{i=-6}^{+6} c(i)E^y_{k,m+i} \qquad (59)$$

where the integral (52) has the coefficients $c(i)$ given by Table IV. For the MRTD simulations, the same $\Delta t$ as for the FDTD simulations has been used, thus the same Gaussian excitation as shown in Fig. 1 has been chosen. Furthermore, exactly the same parameters $\tau$, $\kappa L$, $\beta L$, and $\gamma L$ as for the FDTD simulation have been used. The shift of the maximum of the transmitted pulse by about 500 $\Delta t$ is due to an additional slice of free space in the MRTD mesh between the excitation and the beginning of the nonlinear material. This additional slice of free space separates the excitation and the nonlinear material and thus allows for the use of (48) and (54) without any modifications.

The ABC based on the one-way wave equation and the PML technique have both been applied in the MRTD simulation.

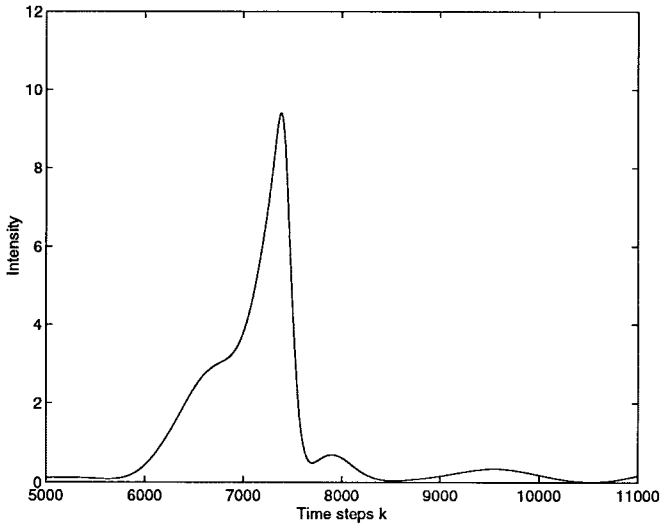


Fig. 7. Transmitted pulse modeled by MRTD without correct modeling of the material transitions.

Since the ABC was found to be highly unstable in the nonlinear simulation, all the results were obtained by terminating the MRTD mesh with PML's. As for the discretization, for the results shown in Fig. 6 a space discretization interval of only $\Delta z = 0.005$ was necessary to obtain the same results as for FDTD. Thus the number of the grid points in the nonlinear material could be reduced from 1000 for FDTD to only 200 for MRTD. Note that using only half of the grid points, the transient pulse starts to be distorted and thus, is not modeled correctly anymore (see Table I). For the absorbing layer, it was found that the thickness could be reduced by a factor of two, which means the results depicted in Fig. 6 were calculated using (28) with $N = 100$ and $\sigma_0 = 0.1$. The execution time for MRTD was about a factor of 1.5 larger than for FDTD which means that the average execution time for one MRTD cell is about a factor of 7.5 larger than the average execution time for one FDTD cell. Fig. 7 illustrates the necessity of modeling the beginning and the end of the nonlinear material sufficiently accurate. While in Fig. 6, the transmitted pulse has been calculated by approximating the integrals $I_{m,m'}$ and $I^{\pm}_{m,m'}$ close to the beginning and the end of the nonlinear material by $9 \times 9$ matrices, the results depicted in Fig. 7 have been obtained by the use of the approximations (41) and (42) only.

## IV. Conclusion

Both FDTD and MRTD schemes for the modeling of nonlinear pulse propagation have been derived and the consequences of the use of nonlocalized instead of localized basis functions have been demonstrated. Furthermore, the correct treatment of the boundary conditions including the modeling of an arbitrary source distribution as well as absorbers for the S-MRTD scheme has been explained in detail. While ABC's based on the analytic Green's function of the one-way wave equation require less computational efforts, they exhibit instabilities in both FDTD and MRTD schemes. Implementing the PML technique in MRTD is straightforward, since for the performance of the absorber it makes no difference whether the conductivity is represented in terms of pulse or scaling functions. In comparison with FDTD, the authors' results suggest that the thickness of the PML in terms of grid points can be reduced by a factor of ten. Thus, in view of 2-D and 3-D MRTD modeling, the PML technique seems to represents the ideal mesh termination for MRTD schemes.

In comparison to the FDTD scheme, the S-MRTD scheme exhibits highly linear dispersion characteristics. These properties allow for a reduction of the mesh size by a factor of five in a 1-D problem while the results are identical. This factor of five is consistent with the results for the linear MRTD modeling. In [4], it has been shown that the MRTD scheme has the capability of providing accurate results for a discretization close to two points per wavelength and close to the Nyquist limit, respectively. In contrast to MRTD, Yee's FDTD scheme is known to provide accurate results only for a discretization of more than ten points per wavelength.

For the given geometry, the execution time for MRTD was about a factor of 1.5 larger than for FDTD indicating that the average execution time for one MRTD cell is about a factor of 7.5 larger than for a FDTD cell. These results suggest the reduction of the mesh size by a factor of 25 and 125 for both 2-D and 3-D problems. In terms of execution time, a reduction of 25/7.5 = 3.33 and 125/7.5 = 16.67 for both 2-D and 3-D modeling may be expected. These numbers confirm the drastic reduction in computer resources observed in the 3-D linear MRTD modeling [3], [4]. Computer savings of one order of magnitude with respect to execution time and two orders of magnitude with respect to the memory requirements make a 3-D MRTD modeling of optical structures feasible.

## References

[1] B. Z. Steinberg and Y. Leviatan, "On the use of wavelet expansions in the method of moments," *IEEE Trans. Antennas Propagat.*, vol. 41, pp. 610–619, May 1993.
[2] K. Sabetfakhri and L. P. B. Katehi, "Analysis of integrated millimeter-wave and submillimeter-wave waveguides using orthonormal wavelet expansions," *IEEE Trans. Microwave Theory Tech.*, vol. 42, pp. 2412–2422, Dec. 1994.
[3] M. Krumpholz and L. P. B. Katehi, "New prospects for time domain analysis," *IEEE Microwave Guided Wave Lett.*, vol. 5, pp. 383–384, Nov. 1995.
[4] ——, "MRTD: New time domain schemes based on multiresolution analysis," *IEEE Trans. Microwave Theory Tech.*, vol. 44, pp. 555–571, Apr. 1996.
[5] K. S. Yee, "Numerical solution of initial boundary value problems involving Maxwell's equations in isotropic media," *IEEE Trans. Antennas Propagat.*, vol. AP-14, pp. 302–307, May 1966.
[6] H. G. Winful, "Pulse compression in optical fiber filters," *Appl. Phys. Lett.*, vol. 46, no. 6, pp. 527–529, Mar. 1985.
[7] R. F. Harrington, *Field Computation by Moment Methods.* Malabar, FL: Krieger, 1982.
[8] M. Krumpholz and P. Russer, "Two-dimensional FDTD and TLM," *Int. J. Num. Modeling*, vol. 7, no. 2, pp. 141–153, Feb. 1993.
[9] ——, "A field theoretical derivation of TLM," *IEEE Trans. Microwave Theory Tech.*, vol. 42, pp. 1660–1668, Sept. 1994.
[10] M. Krumpholz, C. Huber, and P. Russer, "A field theoretical comparison of FDTD and TLM," *IEEE Trans. Microwave Theory Tech.*, vol. 43, pp. 1935–1950, Sept. 1995.
[11] G. Battle, "A block spin construction of ondelettes," *Commun. Math. Phys.*, vol. 110, pp. 601–615, 1987.
[12] P. G. Lemarie, "Ondelettes a localization exponentielle," *J. Math. Pures Appl.*, vol. 67, pp. 227–236, 1988.

[13] S. G. Mallat, "A theory for multiresolution signal decomposition: The wavelet representation," *IEEE Trans. Pattern Anal. Machine Intell.*, vol. 11, pp. 674–693, July 1989.
[14] B. Jawerth and W. Sweldens, "An overview of wavelet based multiresolution analyzes," *SIAM Rev.*, vol. 36, no. 3, pp. 377–412, Sept. 1994.
[15] B. Engquist and A. Majda, "Absorbing boundary conditions for the numerical solution of waves," *Math. Comput.*, vol. 31, no. 139, pp. 629–651, July 1977.
[16] J.-P. Berenger, "A perfectly matched layer for the absorption of electromagnetic waves," *J. Comput. Phys.*, vol. 114, pp. 185–200, 1994.
[17] I. Daubechies, *Ten Lectures on Wavelets.* Philadelphia, PA: Society for Industrial and Applied Mathematics, 1992.

**Michael Krumpholz (M'94),** photograph and biography not available at time of publication.

**Herbert G. Winful (S'73–M'76),** photograph and biography not available at time of publication.

**Linda P. B. Katehi (S'81–M'84–SM'89–F'95)** received the B.S.E.E. degree from the National Technical University of Athens, Athens, Greece, in 1977, and the M.S.E.E. and Ph.D. degrees from the University of California, Los Angeles, (UCLA), in 1981 and 1984, respectively.

In September 1984, she joined the faculty of the Department of Electrical Engineering and Computer Science, University of Michigan, Ann Arbor. She is also an Associate Editor for two IEEE TRANSACTIONS. Her research interests include the development and characterization (both theoretical and experimental) of microwave, millimeter printed circuits, the computer-aided design of VLSI interconnects, the development and characterization of micromachined circuits for millimeter-wave and submillimeter-wave applications, and the development of low-loss lines for Terahertz-frequency applications. She has also been theoretically and experimentally studying various types of uniplanar radiating structures for hybrid-monolithic and monolithic oscillator and mixer designs.

Prof. Katehi has been awarded the IEEE AP-S R. W. P. King (Best Paper Award for a Young Engineer) in 1984, the IEEE AP-S S. A. Schelkunoff Award (Best Paper Award) in 1985, the NSF Presidential Young Investigator Award and an URSI Young Scientist Fellowship in 1987, the Humboldt Research Award and the University of Michigan Faculty Recognition Award in 1994, and the IEEE MTT-S Microwave Prize in 1996. From 1992 to 1995 she had been a member of AP-S ADCOM. She is currently a member of IEEE AP-S, MTT-S, Sigma XI, Hybrid Microelectronics, and URSI Commission D.